

Classification of materials with phonon angular momentum and microscopic origin of angular momentum

Sinisa Coh *Materials Science and Mechanical Engineering, University of California Riverside, California 92521, USA*

(Received 20 August 2023; accepted 3 October 2023; published 13 October 2023)

We group materials into five symmetry classes and determine in which of these classes phonons carry angular momentum in the Brillouin zone, away from a high-symmetry point, line, or plane. In some materials phonons acquire angular momentum via the forces induced by relative displacements of atoms out of their equilibrium positions. However, for other materials, such as ferromagnetic iron, phonon angular momentum arises from the forces induced by relative velocities of atoms. These effects are driven by the spin-orbit interaction.

DOI: [10.1103/PhysRevB.108.134307](https://doi.org/10.1103/PhysRevB.108.134307)

I. INTRODUCTION

A phonon is a quantum of ionic motion in a solid and is characterized by a branch index ν , a crystal momentum \mathbf{q} , and frequency ω . Phonons can also carry angular momentum l [1–4]. Such phonons are characterized by circular, or elliptical, motion of ions. As shown in Ref. [2], each phonon degree of freedom contributes to the energy of the solid by

$$\hbar\omega(n + 1/2)$$

and to the total angular momentum of the solid L by

$$l(n + 1/2).$$

Here n is the Bose-Einstein occupation factor. The magnitude of l^z for a circularly polarized phonon mode moving in the xy plane is $\pm\hbar$, while for the elliptically polarized mode it can have any value between $-\hbar$ and \hbar [5]. In the zero-temperature limit ($n = 0$) each circularly polarized phonon contributes to the angular momentum by one-half of $\pm\hbar$, similar to how each phonon contributes to the energy with one-half of $\hbar\omega$. At elevated temperature, each excited circularly polarized phonon mode contributes $\pm\hbar$ to the total angular momentum, and $\hbar\omega$ to the total energy.

Here we discuss which classes of materials can have phonons with nonzero angular momentum l at the generic nonsymmetric part of the Brillouin zone. Next, for each material class, we discuss the microscopic origin of the angular momentum in the lattice. While for some materials the angular momentum originates within the Born-Oppenheimer approximation [6], in other materials, such as ferromagnetic iron, the phonon angular momentum is acquired only by going beyond that approximation. We present first-principles calculations for both cases.

Phonon angular momentum and the underlying forces that are responsible for its microscopic origin play a crucial role in the diverse range of effect ranging from the phonon Hall effect [7–10] magnetic moment of a phonon [9,11–14], Einstein–de Haas effect [2,15–17], and topological phononic insulators [18] to Dirac materials [19], driven chiral phonons [20–22], and other effects [23].

II. SYMMETRY

We start by using the symmetry arguments to determine in which materials phonons have angular momentum at a generic nonsymmetric part of the Brillouin zone, away from the high-symmetry points, lines, and planes. Restriction to the generic nonsymmetric part of the Brillouin zone greatly simplifies the analysis, as it allows us to only consider the point-group symmetries of the system. Analysis that includes high-symmetry parts of the Brillouin zone would necessarily have to consider the irreducible representation of the magnetic space group associated with each phonon, as at high-symmetry points only modes associated with a specific representation would have phonon angular momentum. Such an analysis is beyond the scope of this manuscript. The second reason for focusing on generic nonsymmetric points is that many physical effects, such as the Einstein–de Haas effect, for example, rely on changes in population of phonons across the entire Brillouin zone. Therefore, in such processes high-symmetry points, lines, or planes are irrelevant as they occupy part of the phonon’s Brillouin zone with no volume, so virtually no phonons correspond to those parts of the Brillouin zone. There are, of course, many other important situations where the high-symmetry points are the only relevant parts of the Brillouin zone. One example is the lowest-order Raman effect [24], where one approximates that the relevant phonons are at a high symmetry point (Brillouin zone origin).

In what follows, when we say that a material has a time-reversal symmetry, we mean that the time-reversal symmetry is contained in the point group of the material. Therefore, we allow for the possibility that in some materials (for example, some antiferromagnets) the actual space group symmetry element consists of time-reversal symmetry followed by a fractional translation of the lattice.

Under these assumptions, we now perform the symmetry analysis of the phonon angular momentum in a material. Inversion operation (\mathcal{P}) of the crystal transforms a phonon (at a generic nonsymmetric point) with angular momentum l and linear momentum \mathbf{q} into a phonon with the same angular

TABLE I. Angular momentum of a phonon at a generic nonsymmetric point (away from high-symmetry points, lines, and planes) in the Brillouin zone in five classes of materials discussed in the text. Angular momentum is allowed in classes III, IV, and V.

Class	Present symmetries			Angular momentum?	Microscopic origin of angular momentum	Examples
	\mathcal{P}	\mathcal{T}	\mathcal{PT}			
I	✓	✓	✓	No		Si, Au
II	×	×	✓	No		Cr ₂ O ₃
III	×	✓	×	Yes	Force-constant matrix $F_{ij}^{\alpha\beta}$	WC, WSe ₂ , HgS, SiO ₂ , Te
IV	✓	×	×	Yes	Velocity-force matrix $G_{ij}^{\alpha\beta}$	Fe, Ni, Co
V	×	×	×	Yes	Both $F_{ij}^{\alpha\beta}$ and $G_{ij}^{\alpha\beta}$	MnGe

momentum but opposite linear momentum,

$$\mathcal{P} : (\mathbf{l}, \mathbf{q}) \longrightarrow (\mathbf{l}, -\mathbf{q}). \quad (1)$$

Similarly, for the time-reversal operation (\mathcal{T}) we have

$$\mathcal{T} : (\mathbf{l}, \mathbf{q}) \longrightarrow (-\mathbf{l}, -\mathbf{q}). \quad (2)$$

Therefore, for an operation \mathcal{PT} that consists of time reversal followed by a spatial inversion, we have

$$\mathcal{PT} : (\mathbf{l}, \mathbf{q}) \longrightarrow (-\mathbf{l}, \mathbf{q}). \quad (3)$$

The product \mathcal{PT} is the only operation of the crystal that leaves \mathbf{q} unchanged at a generic nonsymmetric point of the Brillouin zone. Therefore, from Eq. (3) it follows that if and only if \mathcal{PT} is a symmetry, a phonon at such \mathbf{q} will have a zero angular momentum.

As mentioned earlier, in the derivation above, we are considering \mathbf{q} points away from high-symmetry points, lines, or planes of the Brillouin zone. This is a crucial assumption here, as this guarantees that the phonon under consideration is nondegenerate. Otherwise, if we had a pair of degenerate modes, then the operations \mathcal{P} , \mathcal{T} , or \mathcal{PT} could transform one degenerate phonon mode into another and the analysis above would not hold. Therefore, one can construct a phonon with angular momentum at high-symmetry points in a much wider range of materials, even those with \mathcal{PT} symmetry. As a simple example, graphene [24] has degenerate phonons at $\mathbf{q} = \mathbf{0}$ and one can find a basis in the degenerate subspace of phonons in which individual phonon modes have nonzero angular momentum. Furthermore, it is worth mentioning that in any system, regardless of its symmetries, one can construct a pattern of atomic displacements with angular momentum by taking a linear combination of phonons at \mathbf{q} and $-\mathbf{q}$. In this work we are specifically focusing only on atomic displacements (phonons) that are characterized by a single \mathbf{q} point in the Brillouin zone.

In Table I we summarized five classes of materials with respect to the presence of inversion symmetry (\mathcal{P}), time-reversal symmetry (\mathcal{T}), or their combination (\mathcal{PT}).

Materials in class I are defined as having all three symmetries: \mathcal{P} , \mathcal{T} , and \mathcal{PT} . Since these materials have \mathcal{PT} as one of their symmetries, they can't have a phonon angular momentum at a generic nonsymmetric point in the Brillouin zone. For materials in class II \mathcal{P} and \mathcal{T} are not symmetries, but their product \mathcal{PT} is a symmetry, which leads to the same conclusion. Materials in class III have broken \mathcal{P} and \mathcal{PT} while \mathcal{T} itself is a symmetry. On the other hand, class IV has

broken \mathcal{T} and \mathcal{PT} while \mathcal{P} is a symmetry. In class V all three symmetries are broken.

III. PHONON EQUATION OF MOTION

The dynamics of ions is typically described [6] within the lowest-order Born-Oppenheimer approximation via the force-constant matrix $F_{ij}^{\alpha\beta}$. This matrix describes force induced on the i th atom (in direction α) by a displacement of the j th atom (in direction β). Therefore, equation of motion for the i th nucleus (with mass M_i) is given by

$$-M_i \frac{d^2 x_i^\alpha}{dt^2} = \sum_{j\beta} F_{ij}^{\alpha\beta} x_j^\beta. \quad (4)$$

This description is only approximate, as the true dynamics of nuclei is quantum mechanical, and it therefore cannot be fully described by a classical equation of motion. Within the Born-Oppenheimer approximation the total wave function $\Psi(\mathbf{x}, \mathbf{x}^{\text{elec}})$ for nuclei and electrons is approximated as

$$\Psi(\mathbf{x}, \mathbf{x}^{\text{elec}}) = \psi(\mathbf{x})\phi_{\mathbf{x}}(\mathbf{x}^{\text{elec}}),$$

where ϕ is the instantaneous electronic wave function parametrized by fixed location of nuclei. Using this ansatz within the full Hamiltonian for nuclei and electrons results in an effective Schrodinger equation for nuclear wave function $\psi(\mathbf{x})$. The derivatives of electronic eigenenergies $\partial_{\mathbf{x}} E_{\mathbf{x}}$ associated with electronic wave function ϕ give an effective scalar potential for ions, while the $\langle \phi_{\mathbf{x}} | i \nabla_{\mathbf{x}} | \phi_{\mathbf{x}} \rangle$ acts as an effective vector potential [25–27].

First, we consider the effective scalar potential experienced by nuclei. Expanding around the ground state in terms of small atomic displacements, one obtains the force-constant matrix $F_{ij}^{\alpha\beta}$. Such a force-constant matrix can be computed by first solving a family of electronic Schrodinger equations as a function of all ionic coordinates \mathbf{x} ,

$$H_{\mathbf{x}}\phi_{\mathbf{x}} = E_{\mathbf{x}}\phi_{\mathbf{x}}, \quad (5)$$

and then taking the second derivative of $E_{\mathbf{x}}$ with respect to atomic coordinates,

$$F_{ij}^{\alpha\beta} = \frac{\partial^2 E_{\mathbf{x}}}{\partial x_i^\alpha \partial x_j^\beta}. \quad (6)$$

This approximation can be improved by considering the effective vector potential, as well as higher orders in the expansion (of either scalar or vector potential). In such an expansion the higher-order terms in atomic positions x_j as well as their time

TABLE II. Relationship between various Berry-like objects that depend on either electronic Berry connection \mathcal{A}_k in the reciprocal space (k) or on the ionic Berry connection \mathcal{A}_r in the space of ionic positions (r).

Dimensionality	Electronic Berry-like terms	Mixed electronic-ionic Berry-like terms	Ionic Berry-like terms
1	Polarization $P = \int \mathcal{A}_k dk$	Born effective charge $Z = \int \partial_r \mathcal{A}_k dk$	
2	Anomalous Hall conductivity $\sigma = \int \partial_k \mathcal{A}_k dk$		Velocity-force $G = \int \partial_r \mathcal{A}_r dk$
3	(Component of) magnetoelectric coupling $\theta = \int \mathcal{A}_k \partial_k \mathcal{A}_k dk$		

derivatives can occur. In the lowest order the dynamics is then described by an infinite series of additional terms,

$$\begin{aligned}
 -M_i \frac{d^2 x_i^\alpha}{dt^2} &= \sum_{j\beta} F_{ij}^{\alpha\beta} x_j^\beta + \sum_{j\beta} G_{ij}^{\alpha\beta} \frac{dx_j^\beta}{dt} \\
 &+ \sum_{jk\beta\gamma} H_{ijk}^{\alpha\beta\gamma} x_j^\beta x_k^\gamma + \dots
 \end{aligned} \quad (7)$$

In contrast to the force-constant matrix $F_{ij}^{\alpha\beta}$, the velocity-force constant matrix $G_{ij}^{\alpha\beta}$ cannot be computed from the energies of the electronic Schrodinger equation, but is instead computed from the effective vector potential, which results in

$$G_{ij}^{\alpha\beta} = 2\hbar \text{Im} \left\langle \frac{\partial \phi_{\mathbf{x}}}{\partial x_i^\alpha} \left| \frac{\partial \phi_{\mathbf{x}}}{\partial x_j^\beta} \right. \right\rangle. \quad (8)$$

While this term appears in the so-called Born-Huang approximation [6], it is often ignored as it is assumed to be small. The term G also appears in the quantum-mechanical description of the motion of three identical nuclei on a triangle [28] in an external magnetic field and is seen as an extension of the Aharonov-Bohm effect [29]. In a semiclassical description of atomic motion, as in Eq. (7), the term proportional to G can be thought of as a Lorentz force on a charged particle in an effective magnetic field [30]. Another example where Eq. (8) appears in the literature is in the phonon Hall effect, that was first discovered experimentally [7,31] and then assigned the theoretical origin [32]. In this context the literature refers to Eq. (8) as the Raman spin-phonon interaction. We refer the reader to references in Ref. [33] for a history of the phonon Hall effect.

We incorporate Eq. (8) into equation of motion by using ansatz

$$x_i^\alpha(t) = A M_i^{-1/2} \text{Re}(\xi_i^\alpha e^{i\omega t}). \quad (9)$$

Here A is an arbitrary real constant to be determined later. The phonon eigenvectors (ξ_i^α , defined to be normalized to unity) and frequencies (ω) are then obtained by diagonalizing a generalized eigenvalue problem,

$$\sum_{j\beta} \frac{1}{\sqrt{M_i M_j}} (F_{ij}^{\alpha\beta} + i\omega G_{ij}^{\alpha\beta}) \xi_j^\beta = \omega^2 \xi_i^\alpha. \quad (10)$$

Clearly, if $G = 0$ then the equation above reduces to the well-known problem of finding eigenvalues of a dynamical matrix $F_{ij}^{\alpha\beta} / \sqrt{M_i M_j}$. With $G \neq 0$ the extra term proportional to G has the form of a frequency-dependent correction to the force-constant matrix.

We briefly comment on the mathematical form of Eq. (7) as a Berry curvature in the space of atomic coordinates [30]. In contrast, Berry curvature in the reciprocal space (for fixed atomic coordinates) is related to the off-diagonal σ_{xy} conductivity, appearing in the context of the anomalous Hall effect and integer quantum Hall effect [34,35]. The relationship between different Berry-like quantities is shown in Table II.

IV. MICROSCOPIC ORIGIN OF ANGULAR MOMENTUM

Given the equation of motion Eq. (7) we now come to the question of the origin of the phonon angular momentum.

A. Classes I and III

In class I all three symmetries are present (\mathcal{P} , \mathcal{T} , and \mathcal{PT}), so both $F_{ij}^{\alpha\beta}$ and $G_{ij}^{\alpha\beta}$ terms in Eq. (7) preserve these symmetries and phonons do not have angular momentum at a generic nonsymmetric point in the Brillouin zone.

In class III the time reversal \mathcal{T} is a symmetry, but the inversion symmetry is broken. Therefore, trivially, the inversion symmetry breaking will spill into the force-constant matrix $F_{ij}^{\alpha\beta}$. This can easily be demonstrated on a toy example shown in Fig. 1. (An example of a real solid with broken inversion symmetry is discussed in Ref. [36].) The unit cell there consists of two atoms, indicated with green and orange spheres. If the green atom is exactly in the center of the square formed by orange spheres (left panel), we have inversion symmetry, and therefore force constants (springs) $F_{ij}^{\alpha\beta}$ between green and four orange atoms will all be equal by symmetry. However, if we break the inversion symmetry by displacing the green atom away from the center (middle panel), then two top force constants $F_{ij}^{\alpha\beta}$ will have a different value (thick black line) than the two bottom force constants (thin black line). The fact that $F_{ij}^{\alpha\beta}$ has explicitly broken inversion symmetry means, by our earlier symmetry analysis from Sec. II, that if we solve equation of motion Eq. (7) with such $F_{ij}^{\alpha\beta}$, the resulting phonon eigenvectors will have angular momentum at a generic nonsymmetric point in the Brillouin zone. This mechanism, therefore, will be the source of the phonon angular momentum in class III (and partially in class V as well).

In class III the phonon angular momentum of the same phonon branch at \mathbf{q} must have the opposite sign to that at $-\mathbf{q}$. This follows from Eq. (1), and such phonon band structure is sketched in Fig. 1.

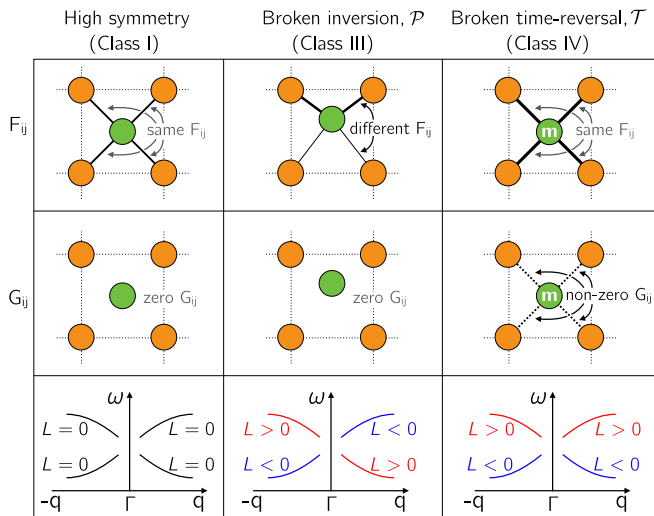


FIG. 1. Sketch of microscopic origins of the phonon angular momentum in a fictitious material with two atoms per unit cell (drawn as green and orange circles). The first column corresponds to material where \mathcal{P} , \mathcal{T} , and \mathcal{PT} symmetries are present. In the second column, inversion (\mathcal{P}) is broken by displacement of the green atom (class III). In the third column, time reversal (\mathcal{T}) is broken by (class IV) magnetism on the green atom (magnetic moment points out of the page). Strengths of force constant matrices $F_{ij}^{\alpha\beta}$ and velocity-force constant matrices $G_{ij}^{\alpha\beta}$ are indicated with black lines in the first and the second row for all three cases. The third row shows sketches of the corresponding phonon band structures and phonon angular momenta in the vicinity of the Brillouin zone origin. Signs of angular momenta for two sketched phonon branches follow from Eqs. (1) and (2). Phonon angular momentum exactly at the origin is excluded from the sketch, as in this work we focus on generic nonsymmetric points of the Brillouin zone only. Phonon angular momentum in the second column (broken inversion, \mathcal{P} , class III) arises from the asymmetric force constants F_{ij} (as sketched in the top panel of the second column). Analogously, in the third column (broken time reversal, \mathcal{T} , class IV) phonon angular momentum arises from the presence of nonzero G_{ij} (as sketched in the middle panel of the third column).

B. Class IV

The situation in class IV is somewhat more complex. In this class of materials, containing ferromagnets such as iron, the inversion symmetry is preserved while the time-reversal symmetry is broken. As a general principle, one would expect that time-reversal breaking in the electronic subsystem must somehow spill into the ionic subsystem, as electrons and ions are coupled. While this is true, the spilling of the time-reversal breaking into ions does not occur in the first term of the expansion in Eq. (7), the force constant matrix $F_{ij}^{\alpha\beta}$, but it does spill into the velocity-force matrix $G_{ij}^{\alpha\beta}$. Let us demonstrate this from the definition of $F_{ij}^{\alpha\beta}$ and $G_{ij}^{\alpha\beta}$.

The force constant $F_{ij}^{\alpha\beta}$ was defined in Eq. (6) as the second derivative of the total energy E_x with respect to atom coordinate. For the solid of any symmetry, the total energy E_x is a scalar that is invariant under the time-reversal operation,

$$\mathcal{T} : E_x \longrightarrow E_x, \quad (11)$$

for any set of atom coordinates \mathbf{x} . Therefore, the derivatives of E_x with respect to \mathbf{x} are also unchanged under \mathcal{T} , so the force-constant matrix is unchanged as well,

$$\mathcal{T} : F_{ij}^{\alpha\beta} \longrightarrow F_{ij}^{\alpha\beta}. \quad (12)$$

This holds regardless of whether the solid itself is in a time-reversal symmetric ground state or not. Therefore, Eq. (12) holds even in a ferromagnet like bulk Fe, or any other materials in class IV. For example, ferromagnetic bulk Fe magnetized along the positive \hat{z} direction will have exactly the same force-constant matrix $F_{ij}^{\alpha\beta}$ as its time-reversed image, where the magnetic moment is reversed to point along the negative \hat{z} axis. This holds true even if spin-orbit interaction, or any other relativistic effect, is included in the calculation.

Since the force-constant matrix $F_{ij}^{\alpha\beta}$ is unaware of the time-reversal symmetry breaking in the solid, any ionic motion in the class IV material that is driven only by the force-constant matrix $F_{ij}^{\alpha\beta}$ will preserve time-reversal symmetry. Therefore, following symmetry analysis from Sec. II, the phonons in class IV material described only by $F_{ij}^{\alpha\beta}$ will not have angular momentum at a generic nonsymmetric point in the Brillouin zone. This same observation can be again made on our toy model from Fig. 1. Imagine that instead of displacing the green atom, we make the green atom magnetic, therefore breaking the time-reversal symmetry in the solid. Magnetization of the green atom is pointing out of the page. Since the distribution of charge on the atom was changed when we made the atom magnetic, one might expect that the resulting force constants between the green and orange atoms will change as well. And they do, but clearly the changes to all four force constants must be equal. More importantly, these four force constants would change by the same amount, regardless of whether the magnetic moment on the green atom in Fig. 1 is pointing in or out of the page. Therefore, adding a magnetic moment to the green atom did not change the symmetry in the force constant matrices $F_{ij}^{\alpha\beta}$, so the underlying phonons did not acquire angular momentum from changes in $F_{ij}^{\alpha\beta}$.

Now let us consider the equation of motion for a solid in class IV that includes the next term in the expansion, the velocity-force constant term $G_{ij}^{\alpha\beta}$. While force-constant matrix is defined in terms of a scalar quantity (total energy E_x) which does not change under time-reversal operation, the velocity-force constant is defined in terms of the electron wave functions [see Eq. (8)], which do change under time reversal. The time-reversal operation, when acting on electron wave functions, is represented by an antiunitary operator $\hat{\mathcal{T}}$. For any two wave functions $|\phi_1\rangle$ and $|\phi_2\rangle$ we define $|\phi'_1\rangle = \hat{\mathcal{T}}|\phi_1\rangle$ and $|\phi'_2\rangle = \hat{\mathcal{T}}|\phi_2\rangle$. For any antiunitary operation, by definition, we have $\langle\phi'_1|\phi'_2\rangle = [\langle\phi_1|\phi_2\rangle]^*$. This gives us

$$\mathcal{T} : \left\langle \frac{\partial\phi_x}{\partial x_i^\alpha} \middle| \frac{\partial\phi_x}{\partial x_j^\beta} \right\rangle \rightarrow \left[\left\langle \frac{\partial\phi_x}{\partial x_i^\alpha} \middle| \frac{\partial\phi_x}{\partial x_j^\beta} \right\rangle \right]^*. \quad (13)$$

Since $G_{ij}^{\alpha\beta}$ from Eq. (8) depends on the imaginary part of this overlap, we conclude that G_{ij} changes sign under time-reversal operation,

$$\mathcal{T} : G_{ij}^{\alpha\beta} \longrightarrow -G_{ij}^{\alpha\beta}. \quad (14)$$

In other words, if a solid has a broken time-reversal symmetry, that breaking will spill into the velocity-force constant matrix $G_{ij}^{\alpha\beta}$, and therefore ionic motion will also experience broken time-reversal symmetry. For example, this means that reversing the direction of the magnetization in bulk ferromagnetic iron from $+\hat{z}$ to $-\hat{z}$ will change the sign of $G_{ij}^{\alpha\beta}$ as well.

[Alternatively, we can demonstrate this point also by considering the expansion in Eq. (7). From this expansion, the $G_{ij}^{\alpha\beta}$ term can be seen as the second derivative of energy, once with respect to atomic position and once with respect to atomic velocity. Therefore, velocity force $G_{ij}^{\alpha\beta}$ changes sign under time reversal as the velocity also changes sign under time reversal. In fact, any term in the equation of motion Eq. (7) with an odd number of time derivatives will change sign under time-reversal symmetry.]

Therefore, the phonon angular momentum in ferromagnetic iron, and any other material in class IV, will originate not from $F_{ij}^{\alpha\beta}$ but from terms with an odd number of time derivatives. Clearly, the dominant contribution will come from $G_{ij}^{\alpha\beta}$, as it is the lowest term in the expansion with the correct number of time derivatives.

In contrast to class III, in class IV the phonon angular momentum of the same phonon branch at \mathbf{q} must have the same sign as that at $-\mathbf{q}$. This follows from Eq. (2) and such phonon band structure is sketched in Fig. 1.

C. Class II

Somewhat more involved is the case of materials in class II. These are antiferromagnets such as Cr_2O_3 , where the inversion symmetry operation \mathcal{P} is centered in between two magnetic Cr atoms with opposing magnetic moments. Therefore, while the spatial inversion \mathcal{P} is broken (as two Cr atoms with opposing magnetic moments are not equivalent), the product \mathcal{PT} of spatial inversion with the time-reversal operation is a symmetry. The presence of \mathcal{PT} symmetry ensures that phonons at a generic nonsymmetric point in the Brillouin zone do not have phonon angular momentum. However, since time reversal itself is broken, the velocity force $G_{ij}^{\alpha\beta}$ is generally nonzero in class II, but this does not induce the phonon angular momentum as $G_{ij}^{\alpha\beta}$ itself must be \mathcal{PT} symmetric.

D. Class V

Finally, we now discuss class V, in which the situation is the simplest from the point of view of symmetry. Now none of the three operations (\mathcal{P} , \mathcal{T} , and \mathcal{PT}) are a symmetry of the systems. Therefore, the phonon angular momentum is now induced both by $F_{ij}^{\alpha\beta}$ and $G_{ij}^{\alpha\beta}$. Furthermore, since there is no symmetry now that would map generic nonsymmetric \mathbf{q} to $-\mathbf{q}$, there is now no relationship between phonon frequency and phonon angular momentum at generic nonsymmetric \mathbf{q} to $-\mathbf{q}$. This is in contrast to the situation in classes III and IV, as sketched in the bottom panels of Fig. 1.

V. EXAMPLE: BROKEN INVERSION SYMMETRY (CLASS III)

Now let us consider phonon angular momentum in a few specific materials, as calculated from the first-principles

approach. First, we will consider material from class III with broken inversion symmetry but with time-reversal symmetry. According to our earlier analysis, phonon angular momentum in this material will originate from the inversion symmetry breaking of the force constant matrix $F_{ij}^{\alpha\beta}$.

As an example of material in class III we considered tungsten-carbide, WC. Its structure can be seen as an alternating series of tungsten and carbon hexagonal sheets. The space group of WC is $\text{P}\bar{6}\text{m}2$ (number 187). This space group does not contain inversion symmetry. The origin of the inversion symmetry breaking is not a displacement of either W or C atoms; it instead originates from the fact that W atom is different from the C atom. If both W and C sites were populated with the same type of atom, the space group would become $\text{P}6_3/\text{mmc}$ (number 194), which does contain inversion symmetry.

Some other interesting materials in class III are α -HgS as studied in Ref. [37], α - SiO_2 studied in Ref. [38], as well as Te studied in Ref. [39].

We computed the phonon band structure of WC within the density functional perturbation theory, as implemented in the QUANTUM-ESPRESSO computer package [40]. We approximate exchange correlation with the Perdew-Burke-Ernzerhof (PBE) approximation [41]. We compute dynamical matrices on a regular $6 \times 6 \times 6$ grid of points and interpolate on a denser grid of points to plot the phonon band structure.

Given a normalized eigenvector ξ_i^α of the dynamical matrix (here α is Cartesian direction and i is atomic index), the phonon angular momentum is given as

$$l^z = 2\hbar \sum_i \text{Im}(\xi_i^x \bar{\xi}_i^y). \quad (15)$$

Similar expressions hold for phonon angular momentum in x and y directions. The derivation of Eq. (15) is given in Refs. [1,2]. Here we only sketch the derivation of the phonon angular momentum in the semiclassical language. Classical atomic displacements of the lattice vibration are given by Eq. (9). If we choose arbitrary constant A in Eq. (9) to equal $\sqrt{2\hbar/\omega}$, then classical energy in the atomic vibration equals $\hbar\omega$, as expected. With this normalization, the computation of the angular momentum of the lattice vibration is now simply

$$l^\alpha = \epsilon^{\alpha\beta\gamma} \sum_{i\beta\gamma} M_i x_i^\beta \frac{dx_i^\gamma}{dt}. \quad (16)$$

If we use now Eq. (9) with $A = \sqrt{2\hbar/\omega}$, we get Eq. (15), in agreement with quantum-mechanical derivation from Refs. [1,2]. (Here $\epsilon^{\alpha\beta\gamma}$ is the Levi-Civita symbol. $\epsilon^{\alpha\beta\gamma} = 1$ for any even perturbation of three indices, $\epsilon^{\alpha\beta\gamma} = -1$ for odd perturbation, and $\epsilon^{\alpha\beta\gamma} = 0$ if any two of the indices are repeating.)

Figure 2 shows calculated phonon band structure, and phonon angular momentum, of tungsten carbide, WC. Phonons with angular momentum along the z axis are indicated with red and blue. Different colors correspond to different signs of the phonon angular momentum l^z . As can be seen from Fig. 2, phonons in class III have opposite angular momentum at \mathbf{q} and $-\mathbf{q}$, which is in agreement with Eq. (2) and the sketch in Fig. 1.

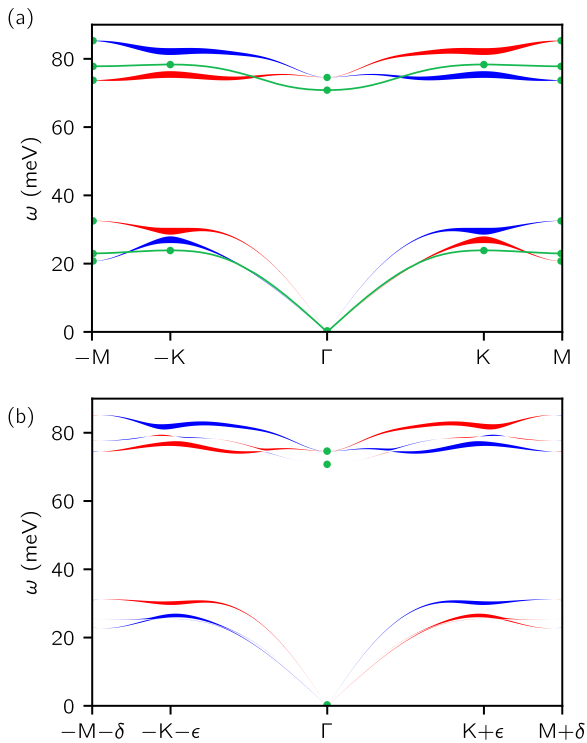


FIG. 2. The phonon band structure of tungsten carbide (class III) along the high-symmetry path (a) in reciprocal space, and along the path that is shifted off the high-symmetry path by around 10% of the reciprocal lattice vector (b). Phonons with positive (negative) angular momentum along the z axis are indicated by red (blue) color. The thickness of the line is proportional to the magnitude of the phonon angular momentum component l^z . The maximum line thickness (at the K points) in the figure corresponds to the circularly polarized phonon mode with $l = \pm\hbar$. Phonons at high-symmetry lines and points that by symmetry have $l^z = 0$ are indicated with a green line and dot.

Phonons that have $l^z = 0$ by symmetry are indicated with a green line or circle. As can be seen from Fig. 2(a), there are two phonon branches, indicated with a green line, that have $l^z = 0$ along the entire Γ - K - M path. Furthermore, all phonons have $l^z = 0$ at inversion symmetry invariant M point, but only two phonons have $l^z = 0$ at the K point. At the Γ point one can choose a basis of phonon modes so that $l^z = 0$ for all phonon branches. However, for the doubly degenerate modes at the Γ point one can choose a basis so that $l^z \neq 0$. Figure 2(b) shows phonon band structure on a straight line in the phonon Brillouin zone which passes only near K and M points, but never goes through K and M . This path is chosen so that it avoids high-symmetry points, lines, and planes (except for origin, Γ). As can be seen from Fig. 2(b), all six phonons now have nonzero l^z along the entire path (except for Γ), in agreement with the discussion in Sec. II.

VI. EXAMPLE: BROKEN TIME-REVERSAL SYMMETRY (CLASS IV)

Now we consider the example of a material from class IV. We will consider ferromagnetic bcc iron, as it is one of

the simplest materials in this class. We computed the force-constant (dynamical) matrix using the density functional perturbation theory, as implemented in the QUANTUM-ESPRESSO computer package [40], within the PBE approximation [41]. We compute dynamical matrices on a regular $4 \times 4 \times 4$ grid of \mathbf{q} points in the conventional unit cell with two Fe atoms per cell (this would correspond to effectively $5 \times 5 \times 5$ grid of \mathbf{q} points in the primitive unit cell).

Since bcc iron has inversion symmetry, the phonon angular momentum has to arise from the velocity-force constant matrix $G_{ij}^{\alpha\beta}$, as discussed earlier. We evaluate the interband part of $G_{ij}^{\alpha\beta}$ starting from Eq. (8). Since this expression includes only the occupied states, we can express $G_{ij}^{\alpha\beta}$ in terms of one-electron orbitals ϕ_{kn} and occupations f_{kn} ,

$$G_{ij}^{\alpha\beta} = 2\hbar \frac{1}{N_k} \sum_k \text{Im} \sum_n f_{kn} \left\langle \frac{\partial \phi_{kn}}{\partial x_i^\alpha} \left| \frac{\partial \phi_{kn}}{\partial x_j^\beta} \right. \right\rangle. \quad (17)$$

We compute the real-space Berry curvature by the finite-difference approach. Let us denote with ϕ_{kn} a one-electron orbital for a system in which all atoms are at ground state locations and $\phi_{kn}^{i\alpha}$ is the one where the i th atom is displaced by Δ in Cartesian direction α . The expression for real-space Berry curvature then becomes

$$G_{ij}^{\alpha\beta} = \frac{\hbar}{\Delta^2} \frac{1}{N_k} \sum_k \text{Im} \sum_{mno} [(f_{km}^{1/6} \langle \phi_{km} | \phi_{kn}^{i\alpha} \rangle f_{kn}^{1/6}) \times (f_{kn}^{1/6} \langle \phi_{kn}^{i\alpha} | \phi_{ko}^{j\beta} \rangle f_{ko}^{1/6}) (f_{ko}^{1/6} \langle \phi_{ko}^{j\beta} | \phi_{kp} \rangle f_{kp}^{1/6})]. \quad (18)$$

Clearly, this expression will revert to Eq. (17) in the limit of occupations at zero temperature [in the zero-temperature limit, one can disregard exponents on occupation factors in Eq. (17)]. However, this expression has an advantage in that, unlike Eq. (17), it does not assume that states can be labeled with the consistent band label as atoms are displaced. In Eq. (18) the sum is done over all states, and since it is manifestly gauge invariant, it therefore does not depend on the labeling of bands.

We computed Eq. (18) from first principles. We first compute fully relativistic (including spin-orbit) ground state wave functions (ϕ_{kn}) of bulk bcc iron in a ferromagnetic state. Next we construct a $2 \times 2 \times 2$ supercell of the conventional unit cell (this supercell contains 16 Fe atoms, as there are two atoms of Fe per one conventional unit cell). Magnetic moment is set to point along the z axis, which is the easy axis of the magnetic anisotropy. Next, we rigidly displace one of the Fe atoms in the supercell (labeled with $i = 1$) along the $\alpha = x$ direction and repeat the calculation of the electron orbitals (we label these as $\phi_{kn}^{i=1, \alpha=x}$). We repeat the same calculation for a displacement of atoms along the $\alpha = y$ direction. There is no need to displace atoms in the z direction, as $G_{ij}^{\alpha\beta} = 0$ by symmetry when either α or β are z (we also confirmed this by a direct calculation). The magnitude of the atomic displacements in the x or y direction is 6×10^{-3} Å. There is no need to compute wave functions for the displacements of the remaining $16 - 1 = 15$ atoms in the supercell, as those

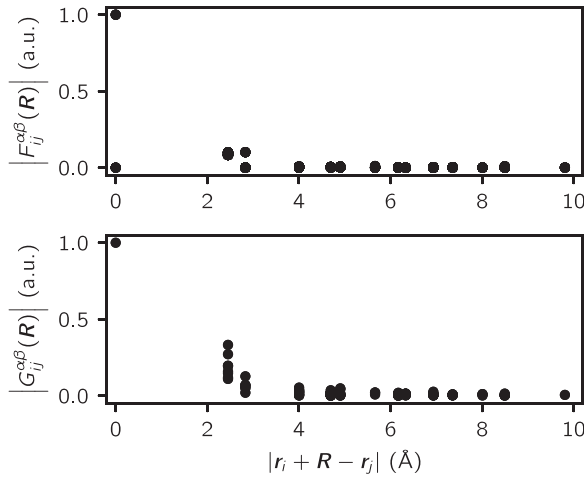


FIG. 3. Norm of the Fourier transform of force-constant matrix $F_{ij}^{\alpha\beta}$ and velocity-constant matrix $G_{ij}^{\alpha\beta}$ as a function of distance between atoms.

can be obtained trivially by real-space translation of the wave function inside the supercell.

Next we obtain the needed $G_{ij}^{\alpha\beta}$ elements by directly computing the overlaps between the wave functions as given in Eq. (18). To get better spatial resolution of $G_{ij}^{\alpha\beta}$ we also perform Wannier interpolation [42] to an effective $4 \times 4 \times 4$ supercell (containing in total 128 Fe atoms). Figure 3 shows that both the force-constant matrix $F_{ij}^{\alpha\beta}$ and the velocity-force matrix $G_{ij}^{\alpha\beta}$ decay very quickly in the real space.

Results for the phonon dispersion in iron, including the effects of the velocity-force constant matrix $G_{ij}^{\alpha\beta}$, are shown in Fig. 4. The addition of the velocity-force constant term introduces a small gap opening between the two transverse acoustic branches. In the vicinity of the gap opening, the phonons are fully circularly polarized. (We computed phonon angular momentum using Eq. (15), which is valid in class IV and V as long as $G_{ij}^{\alpha\beta}$ is small [43].) These regions with nonzero phonon angular momentum are indicated with a yellow color in Fig. 4. Since without the velocity-force term the transverse phonons are exactly degenerate along the $q_x = q_y = 0$ line, the velocity-force constant term introduces fully quantized angular momentum in the vicinity of the line regardless of its strength. Of course, with stronger spin-orbit coupling we expect that the induced velocity force will be larger. For example, the phonon gap opening in CeF_3 [44]—which likely originates from the same microscopic mechanism, as discussed in Ref. [2]—is about 25 cm^{-1} , which is 6% of the phonon frequency. Recent theoretical work on a different material, ferromagnetic CrI_3 , finds significantly smaller phonon splitting, since the relevant phonon frequency is much lower than the acoustic magnon frequency at Γ [45].

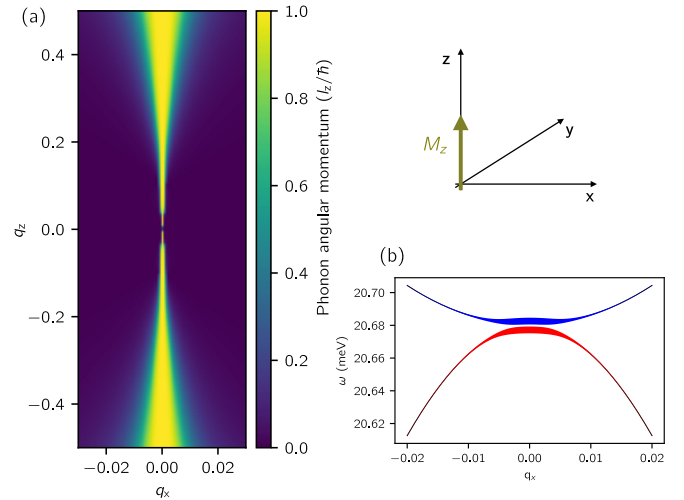


FIG. 4. Phonon angular momentum of ferromagnetic bcc iron (class IV). Phonon wave vector is defined in the conventional unit cell (containing two iron atoms). Phonon wave vector component q_y is set to zero. (a) Yellow indicates regions of the Brillouin zone in which two nearly degenerate transverse acoustic phonons are circularly polarized ($l = \pm\hbar$) due to the velocity-force term $G_{ij}^{\alpha\beta}$. Phonons in purple regions have a negligible amount of phonon angular momentum. The magnetization of iron is pointing along the z axis. (b) Cut through the phonon Brillouin zone (defined by $q_y = 0$ and $q_z = 0.4$) using the same coloring convention for the phonon angular momentum as in Fig. 2.

VII. CONCLUSION

We performed symmetry analysis to understand which materials can or cannot have phonons with angular momentum at generic nonsymmetric parts of the Brillouin zone (away from high-symmetry point, line, or plane). All materials fall into one of the five classes, depending on whether \mathcal{P} , \mathcal{T} , and \mathcal{PT} are symmetries or not. Here, spatial inversion symmetry is denoted as \mathcal{P} while time reversal is denoted as \mathcal{T} . The time-reversal breaking in the phonon dynamics does not occur in the force-constant matrices. Instead, one must go to the next term in the expansion, the velocity-force constant matrix $G_{ij}^{\alpha\beta}$. The $G_{ij}^{\alpha\beta}$ measures force on atom i induced by velocity, not displacement, of atom j . These effects will be relevant not only for phonon angular momentum in class IV, but also for any other effect that depends on time-reversal breaking in phonons, such as phonon Hall effect, magnetic moment of a phonon, and Einstein–de Haas effect.

ACKNOWLEDGMENTS

This work was supported by Grant No. NSF DMR-1848074. I acknowledge discussions with Richard Wilson, Massimiliano Stengel, and Cyrus Dreyer.

[1] A. G. McLellan, *J. Phys. C* **21**, 1177 (1988).
 [2] L. Zhang and Q. Niu, *Phys. Rev. Lett.* **112**, 085503 (2014).
 [3] L. Zhang and Q. Niu, *Phys. Rev. Lett.* **115**, 115502 (2015).

[4] H. Zhu, J. Yi, M.-Y. Li, J. Xiao, L. Zhang, C.-W. Yang, R. A. Kaindl, L.-J. Li, Y. Wang, and X. Zhang, *Science* **359**, 579 (2018).

- [5] On general quantum mechanical principles, for any rotationally invariant solid one can find a basis of eigenstates with an expectation value of angular momentum that is an integer multiple of \hbar . However, this is not the case for a solid with periodic boundary condition, as periodic boundary condition breaks the rotational symmetry of the system.
- [6] M. Born and K. Huang, *Dynamical Theory of Crystal Lattices* (Clarendon, Oxford, 1954).
- [7] C. Stroh, G. L. J. A. Rikken, and P. Wyder, *Phys. Rev. Lett.* **95**, 155901 (2005).
- [8] G. Grissonnanche, S. Thériault, A.ourgout, M.-E. Boulanger, E. Lefrançois, A. Ataei, F. Laliberté, M. Dion, J.-S. Zhou, S. Pyon, T. Takayama, H. Takagi, N. Doiron-Leyraud, and L. Taillefer, *Nat. Phys.* **16**, 1108 (2020).
- [9] S. Park and B.-J. Yang, *Nano Lett.* **20**, 7694 (2020).
- [10] B. Flebus and A. H. MacDonald, [arXiv:2205.13666](https://arxiv.org/abs/2205.13666).
- [11] D. M. Juraschek, M. Fechner, A. V. Balatsky, and N. A. Spaldin, *Phys. Rev. Mater.* **1**, 014401 (2017).
- [12] D. M. Juraschek and N. A. Spaldin, *Phys. Rev. Mater.* **3**, 064405 (2019).
- [13] Y. Ren, C. Xiao, D. Saparov, and Q. Niu, *Phys. Rev. Lett.* **127**, 186403 (2021).
- [14] G. Xiong, Z. Yu, and L. Zhang, *Phys. Rev. B* **105**, 024312 (2022).
- [15] D. A. Garanin and E. M. Chudnovsky, *Phys. Rev. B* **92**, 024421 (2015).
- [16] J. J. Nakane and H. Kohno, *Phys. Rev. B* **97**, 174403 (2018).
- [17] S. R. Tauchert, M. Volkov, D. Ehberger, D. Kazenwadel, M. Evers, H. Lange, A. Donges, A. Book, W. Kreuzpaintner, U. Nowak, and P. Baum, *Nature (London)* **602**, 73 (2022).
- [18] C. Kane and T. Lubensky, *Nat. Phys.* **10**, 39 (2014).
- [19] L.-H. Hu, J. Yu, I. Garate, and C.-X. Liu, *Phys. Rev. Lett.* **127**, 125901 (2021).
- [20] D. M. Juraschek, P. Narang, and N. A. Spaldin, *Phys. Rev. Res.* **2**, 043035 (2020).
- [21] R. M. Geilhufe, V. Juričić, S. Bonetti, J.-X. Zhu, and A. V. Balatsky, *Phys. Rev. Res.* **3**, L022011 (2021).
- [22] R. M. Geilhufe and W. Hergert, *Phys. Rev. B* **107**, L020406 (2023).
- [23] M. Hamada, E. Minamitani, M. Hirayama, and S. Murakami, *Phys. Rev. Lett.* **121**, 175301 (2018).
- [24] Y. Tatsumi, T. Kaneko, and R. Saito, *Phys. Rev. B* **97**, 195444 (2018).
- [25] J. Moody, A. Shapere, and F. Wilczek, *Phys. Rev. Lett.* **56**, 893 (1986).
- [26] A. Abedi, N. T. Maitra, and E. K. U. Gross, *Phys. Rev. Lett.* **105**, 123002 (2010).
- [27] T. Qin, J. Zhou, and J. Shi, *Phys. Rev. B* **86**, 104305 (2012).
- [28] C. A. Mead and D. G. Truhlar, *J. Chem. Phys.* **70**, 2284 (1979).
- [29] C. Alden Mead, *Chem. Phys.* **49**, 23 (1980).
- [30] R. Resta, *J. Phys.: Condens. Matter* **12**, R107 (2000).
- [31] A. V. Inyushkin and A. N. Taldenkov, *JETP Lett.* **86**, 379 (2007).
- [32] L. Sheng, D. N. Sheng, and C. S. Ting, *Phys. Rev. Lett.* **96**, 155901 (2006).
- [33] L. Zhang, J. Ren, J.-S. Wang, and B. Li, *J. Phys.: Condens. Matter* **23**, 305402 (2011).
- [34] G. Sundaram and Q. Niu, *Phys. Rev. B* **59**, 14915 (1999).
- [35] F. D. M. Haldane, *Phys. Rev. Lett.* **93**, 206602 (2004).
- [36] K. Moseni, R. B. Wilson, and S. Coh, *Phys. Rev. Mater.* **6**, 104410 (2022).
- [37] K. Ishito, H. Mao, Y. Kousaka, Y. Togawa, S. Iwasaki, T. Zhang, S. Murakami, J. ichiro Kishine, and T. Satoh, *Nat. Phys.* **19**, 35 (2023).
- [38] H. Ueda, M. García-Fernández, S. Agrestini, C. P. Romao, J. van den Brink, N. A. Spaldin, K.-J. Zhou, and U. Staub, *Nature (London)* **618**, 946 (2023).
- [39] H. Chen, W. Wu, J. Zhu, Z. Yang, W. Gong, W. Gao, S. A. Yang, and L. Zhang, *Nano Lett.* **22**, 1688 (2022).
- [40] P. Giannozzi, S. Baroni, N. Bonini, M. Calandra, R. Car, C. Cavazzoni, D. Ceresoli, G. L. Chiarotti, M. Cococcioni, I. Dabo, A. D. Corso, S. de Gironcoli, S. Fabris, G. Fratesi, R. Gebauer, U. Gerstmann, C. Gougoussis, A. Kokalj, M. Lazzeri, L. Martin-Samos *et al.*, *J. Phys.: Condens. Matter* **21**, 395502 (2009).
- [41] J. P. Perdew, K. Burke, and M. Ernzerhof, *Phys. Rev. Lett.* **77**, 3865 (1996).
- [42] N. Marzari, A. A. Mostofi, J. R. Yates, I. Souza, and D. Vanderbilt, *Rev. Mod. Phys.* **84**, 1419 (2012).
- [43] Reference [46] derives phonon angular momentum by carefully considering the difference between the kinetic and canonical momentum. In classes IV and V this distinction leads to a small correction to the phonon angular momentum, proportional to $(\omega - \omega_0)/\omega_0$. Here ω_0 is the phonon frequency when all $G_{ij}^{\alpha\beta}$ in Eq. (10) are set to zero.
- [44] G. Schaack, *Solid State Commun.* **17**, 505 (1975).
- [45] J. Bonini, S. Ren, D. Vanderbilt, M. Stengel, C. E. Dreyer, and S. Coh, *Phys. Rev. Lett.* **130**, 086701 (2023).
- [46] D. Saparov, B. Xiong, Y. Ren, and Q. Niu, *Phys. Rev. B* **105**, 064303 (2022).